Langmuir
Article
pubs.acs.org/Langmuir

Theoretical Framework for Nanoparticle Reactivity as a Function of Aggregation State

Ernest M. Hotze,[†,‡] Jean-Yves Bottero,[‡] and Mark R. Wiesner*[,†]

[†]*Department of Civil and Environmental Engineering, Duke University, Durham, North Carolina 27708-0287, and* [‡]*CEREGE, University Aix-Marseille, Aix-en-Provence, France*

Received April 17, 2009. Revised Manuscript Received April 15, 2010

Theory is developed that relates the reactivity of nanoparticles to the structure of aggregates they may form in suspensions. This theory is applied to consider the case of reactive oxygen species (ROS) generation by photosensitization of C_{60} fullerenes. Variations in aggregate structure and size appear to account for an apparent paradox in ROS generation as calculated using values for the photochemical kinetics of fullerene (C_{60}) and its hydroxylated derivative, fullerol ($C_{60}(OH)_{22-24}$) and assuming that structure varies between compact and fractal objects. A region of aggregation-suppressed ROS production is identified where interactions between the particles in compact aggregates dominate the singlet oxygen production. Intrinsic kinetic properties dominate when aggregates are small and/or are characterized by low fractal dimensions. Pseudoglobal sensitivity analysis of model input variables verifies that fractal dimension, and by extension aggregation state, is the most sensitive model parameter when kinetics are well-known. This theoretical framework qualitatively predicts ROS production by fullerol suspensions 2 orders of magnitude higher compared with aggregates of largely undifferentiated C_{60} despite nearly an order of magnitude higher quantum yield for the undifferentiated C_{60} based on measurements for single molecules. Similar to C_{60}, other primary nanoparticles will exist as aggregates in many environmental and laboratory suspensions. This work provides a theoretical basis for understanding how the structure of nanoparticle aggregates may affect their reactivity.

Introduction

Nanoparticles are characterized by length scales that are larger than the atomic scale, and yet small enough that novel phenomena such as quantum effects, surface plasmon resonance, or superparamagnetism confer unique properties on the nanoparticle compared with the same material present in a larger "bulk" format. Within the gray zone between the atomic and bulk scales, the properties of nanomaterials may be expected to change due to the formation of nanoparticle clusters to an extent that is intermediate between those when atoms form molecules and colloidal particles aggregate. Indeed, certain cases of nanoparticle aggregation have been described by analogy to atomic theory, where the thermodynamic stability of aggregates can be predicted by "superatomic electronic theory" in which nanoparticle aggregates have a core−shell structure.[1]

In this work, we develop a theoretical framework for describing the impact of aggregate structure on the reactivity of nanoparticles in suspension. Aggregation has been shown to decrease the dissolution of lead sulfide nanoparticles due to the confined space between the particles causing limited diffusion of water to the surface.[2] Aggregation also decreases dechlorination rates of carbon tetracholoride, a common groundwater contaminant, using maghemite nanoparticles[3] and has been demonstrated to affect the photogenerated reactive oxygen species (ROS) that are produced by fullerene derivatives.[4] Our theory is illustrated for the latter case of fullerene aggregates where reactivity takes the form of C_{60} molecule photosensitization.

The theory resolves the apparent paradox between observations of ROS production by aqueous suspensions of fullerenes and the high quantum yields observed for ROS production by C_{60}[4] in comparison to those estimated for highly functionalized C_{60} observed in organic solutions.[5] As first observed by Pickering and Wiesner[6] and later replicated by others,[7] aggregates of fullerol in aqueous suspensions produce relatively large amounts of ROS[5,6,8,9] when irradiated by UV light while aggregates of the undifferentiated C_{60} produce little to no detectable ROS. We have hypothesized a direct link between structures of fullerene aggregates and ROS production kinetics.[9] The theory developed in the current work predicts qualitative trends in C_{60} and fullerol photochemistry that are consistent with observations and may be similarly applicable by extension to other systems where the reactivity of nanoparticle surfaces is affected by close proximity to other nanoparticles due to aggregation or deposition. This fullerene system is but one illustration of how the reactivity of

*To whom correspondence should be addressed. E-mail: wiesner@duke.edu. Telephone: 919-660-5292.

(1) Walter, M.; Akola, J.; Lopez-Acevedo, O.; Jadzinsky, P. D.; Calero, G.; Ackerson, C. J.; Whetten, R. L.; Gronbeck, H.; Hakkinen, H. A unified view of ligand-protected gold clusters as superatom complexes. *Proc. Natl. Acad. Sci. U.S.A.* **2008**, 105.

(2) Liu, J.; Aruguete, D. M.; Jinschek, J. R.; Rimstidt, J. D.; Hochella, M. F. The non-oxidative dissolution of galena nanocrystals: Insights into mineral dissolution rates as a function of grain size, shape, and aggregation state. *Geochim. Cosmochim. Acta* **2008**, 72.

(3) Vikesland, P. J.; Heathcock, A. M.; Rebodos, R. L.; Makus, K. E. Particle size and aggregation effects on magnetite reactivity toward carbon tetrachloride. *Environ. Sci. Technol.* **2007**, *41*, 5277.

(4) Arbogast, J. W.; Darmanyan, A. P.; Foote, C. S.; Rubin, Y.; Diederich, F. N.; Alvarez, M. M.; Anz, S. J.; Whetten, R. L. Photophysical properties of C_{60}. *J. Phys. Chem.* **1991**, *95*, 11.

(5) Mohan, H.; Palit, D. K.; Mittal, J. P.; Chiang, L. Y.; Asmus, K. D.; Guldi, D. M. Excited states and electron transfer reactions of $C_{60}OH_{18}$ in aqueous solution. *J. Chem. Soc., Faraday Trans.* **1998**, *94*, 359.

(6) Pickering, K. D.; Wiesner, M. R., Fullerol-sensitized production of reactive oxygen species in aqueous solution. *Environ. Sci. Technol.* **2005**, *39*, 1359.

(7) Lee, J.; Fortner, J. D.; Hughes, J. B.; Kim, J. H., Photochemical production of reactive oxygen species by C_{60} in the aqueous phase during UV irradiation. *Environ. Sci. Technol.* **2007**, *41*, 2529.

(8) Mohan, H.; Chiang, L. Y.; Mittal, J. P. Radiation Chemical Investigations on Aqueous Solutions of $C_{60}OH_{18}$. *Res. Chem. Intermed.* **1997**, *23*, 403.

(9) Hotze, E. M.; Labille, J.; Alvarez, P.; Wiesner, M. R. Mechanisms of photochemistry and reactive oxygen production by fullerene suspensions in water. *Environ. Sci. Technol.* **2008**, *42*, 4175.

primary nanoparticles can be transformed significantly by their aggregation and how, given estimates of kinetics and aggregation state (size and fractal dimension), these transformations can be estimated.

Aggregation and Fractal Dimension

Principles from fractal geometry have been used previously to model aggregation and deposition of particles and fouling layers in membranes.[10−13] Self-similar fractal objects exhibit a morphology that is statistically scale-invariant.[14] The self-similar nature of objects described by fractal dimension (D) is useful in that it provides a more fundamental descriptor of aggregate properties described by power-law relationships, compared with properties such as density or porosity that may vary with scale. The density of a fractal particle aggregate (volume of primary particles per volume of aggregate) can be expressed as

$$\rho_f \approx {d_f}^{D-3} \tag{1}$$

In the current context, ρ_f is the number density of C_{60} molecules in an aggregate (or floc) of diameter d_f. Accordingly, the valid range for the fractal dimension is $1 \leq D \leq 3$ where 1 represents a linear aggregate (C_{60} cages lined up one after another) and 3 represents a compact object with a Euclidean dimension of 3.

Taking density as the measure of the local concentration of nanoparticles within each individual aggregate, eq 2 is derived calculating the number of fullerene cages per aggregate or "floc" (N_F) and subsequently local reaction rates within each floc.

$$N_F = \left(\frac{d_f}{d_p}\right)^D \tag{2}$$

Here, d_p is the diameter of the primary particle. These reaction rates will differ from those occurring based on the assumption of a homogeneous distribution in the suspension as the local concentrations of fullerenes in the aggregate may be many orders of magnitude greater than those found in the bulk. However, due to reduced degrees of freedom, the activity of these molecules will also likely be reduced in the aggregate. The appropriate metric for aggregate diameter (twice the radius of gyration, the hydrodynamic diameter, etc.) is set-aside for the purposes of this discussion.

From eq 2, an expression for the concentration $[C_{60}]_F$ of primary cages within the volume of a single floc is derived:

$$[C_{60}]_F = {N_F}^{1-\frac{3}{D}} \frac{6}{\pi} \frac{1}{{d_p}^3 N_A} \tag{3}$$

where Avogadro's number, N_A, converts number to molar concentrations.

In addition to the concentration of C_{60} cages in a floc ($[C_{60}]_F$), porosity (ε) and fraction of cages at the surface of the aggregate (f_s) can be estimated knowing the fractal dimension and aggregate diameter. Aggregate porosity can be expressed as 1 minus the density:

$$\varepsilon = 1 - \frac{[C_{60}]_F}{\beta} \tag{4}$$

where β is a conversion factor, based on C_{60} (or fullerol) density, that converts molar concentration to volume fraction.

Cages buried within a dense aggregate are anticipated to be less susceptible to excitation due to partial illumination. In this model, the average efficiency of C_{60} illumination throughout the aggregate is assumed to be proportional to the fraction of C_{60} near the surface of aggregates (f_s):

$$f_s = {N_F}^{\frac{2.0}{D}-1} \tag{5}$$

As D approaches a value of 2.0, or as $N_F \rightarrow 1$, virtually all of the C_{60} is present on the aggregate surface and f_s approaches unity.

Structures of Fullerene Aggregates Have a Fractal Character

We have previously shown[9,15] that aqu/nC_{60} typically ranges in size from 20 nm to several hundred nanometers in diameter and is composed of highly ordered, crystal-like assemblies of C_{60}. In contrast, fullerol aggregates have a more amorphous, disordered structure as evidenced by the lack of sharp diffraction peaks in X-ray diffraction measurments[9,16] and a smaller number-average diameter. These observations are consistent with a top-down formation of aqu/nC_{60} resulting from a breakup of the initial crystalline C_{60} powder versus the bottom-up formation of fullerol aggregates via a diffusion-limited assembly of the hydroxylated material when added to water.

Evidence from literature also indicates that fullerenes aggregate in a fractal manner. For example, Ying et al.[17] demonstrated that bifunctionalized fullerenes aggregate in a fractal manner, while transmission electron microscopy images from publications by Brant et al.[16] and Vileno et al.[18] also show a fractal-like structure for these aggregates.

Kinetics of Photosensitization

Fullerene molecules are photosensitizers, capable of transferring light energy to chemical oxidation potential in the form of ROS. Singlet oxygen production via photosensitization by individual C_{60} molecules in organic solvent proceeds with a quantum yield near unity,[4] indicating little to no loss of energy between initial photosensitization and formation of its triplet excited state ($^3C_{60}$). When the photosensitized molecule transfers energy directly to an oxygen molecule, ROS formation may occur via a type II pathway primarily resulting in singlet oxygen ($^1O_2$). Further details on kinetic pathways of fullerenes photosensitization are provided in the Supporting Information.

An important difference between C_{60} in water and in organic solvents is the tendency of C_{60} to form stable colloidal aggregates

(10) Jiang, Q.; Logan, B. E., Fractal dimensions of aggregates determined from steady-state size distributions. *Environ. Sci. Technol.* **1991**, *25*, 2031.
(11) Wiesner, M. R. Kinetics of aggregate formation in rapid mix. *Water Res.* **1992**, *26*, 379.
(12) Veerapaneni, S.; Wiesner, M. R. Hydrodynamics of fractal aggregates with radially varying permeability. *J. Colloid Interface Sci.* **1996**, 177.
(13) Tarabara, V. V.; Pierrisnard, F.; Parron, C.; Bottero, J. Y.; Wiesner, M. R. Morphology of deposits formed from chemically heterogeneous suspensions: Application to membrane filtration. *J. Colloid Interface Sci.* **2002**, *256*, 367.
(14) Bunde, A.; Havlin, S. *Fractals and disordered systems*; Springer-Verlag: Berlin; New York, 1991; p 350.
(15) Brant, J. A.; Labille, J.; Bottero, J. Y.; Wiesner, M. R. Characterizing the impact of preparation method on fullerene cluster structure and chemistry. *Langmuir* **2006**, *22*, 3878.
(16) Brant, J. A.; Labille, J.; Robichaud, C. O.; Wiesner, M. Fullerol cluster formation in aqueous solutions: Implications for environmental release. *J. Colloid Interface Sci.* **2007**, *314*, 281.
(17) Ying, Q.; Zhang, J.; Liang, D.; Nakanishi, W.; Isobe, H.; Nakamura, E.; Chu, B. Fractal Behavior of Functionalized Fullerene Aggregates. I. Aggregation of Two-Handed Tetraaminofullerene with DNA. *Langmuir* **2005**, *21*, 9824.
(18) Vileno, B.; Marcoux, P. R.; Lekka, M.; Sienkiewicz, A.; Feher, I.; Forro, L. Spectroscopic and photophysical properties of a highly derivatized C_{60} fullerol. *Adv. Funct. Mater.* **2006**, *16*, 120.

in water. We have previously reported on the relative ROS production by fullerol and aqu/nC$_{60}$ in water.[6,19] We seek to more fundamentally understand why C$_{60}$ aggregates in the polar aqueous environment exhibit suppressed photochemical activity in comparison with fullerol when their intrinsic properties indicate that C$_{60}$ should be the more active of the two molecules. The apparent paradox between quantum yields and ROS production can be understood in the context of the structural differences between the aggregates formed by these two fullerenes, and underscores the importance of the local concentration of fullerenes within the aggregate as reflected by aggregate structure in determining nanoparticle reactivity.

Theory for fullerene reactivity as aggregate suspensions, therefore, begins with an expression for the rate of change of triplet state C$_{60}$ concentrations within an aggregate averaged over the entire aggregate and can be written as

$$\frac{d[T_1]}{dt} = f_s k_{GT}[S_0] - k_{SQ}[T_1][S_0] - 1/2k_{TT}[T_1]^2 - \varepsilon k_\Delta[T_1][O_2(^3\Sigma)] \quad (6)$$

Porosity (ε) is calculated from eq 4 and gives the ratio of free to occupied space in the aggregate. Since all C$_{60}$ molecules within the aggregate are assumed to be in either the ground or triplet state, it follows that the sum of triplet state and ground state molecules is the total number molecules ($[T_1] + [S_0] = [C_{60}]_F$) which is in turn given by eq 3. Expressing $[S_0]$ in eq 6 as $[C_{60}]_F - [T_1]$, assuming that ground state oxygen ($O_2(^3\Sigma)$) is constant in the suspension and within the aggregate (i.e., no mass transfer limitations for oxygen), and further assuming steady state (SS), a quadratic equation in $[T_1]_F$, the concentration of C$_{60}$ triplets per volume of aggregate, is obtained

$$[T_1]_F = f_s k_{GT} + [C_{60}]_F k_{SQ} + \varepsilon k_\Delta[O_2(^3\Sigma)] - \left[\sqrt{\left(f_s k_{GT} + [C_{60}]_F k_{SQ} + \varepsilon k_\Delta[O_2(^3\Sigma)]\right)^2 - 4[C_{60}]_F f_s k_{GT}(k_{SQ} - 0.5k_{TT})}\right] \Big/ \left[2(k_{SQ} - 0.5k_{TT})\right] \quad (7)$$

As fractal dimension and/or aggregate size becomes small, a larger fraction of the C$_{60}$ are present on the surface of aggregates where there are fewer mass transport limitations and reduced interactions with adjacent cages. Moreover, as the number of C$_{60}$ cages within an aggregate approaches a value of 1, fractal geometry can no longer be assumed. The asymptotic solution in this case is that of the standard case for freely suspended entities yielding the following expression for the steady state triplet concentration in the suspension ($[T_1]_S$):

$$[T_1]_S = k_{GT} + f_s\left(\frac{N_{BF}}{N_A}\right)k_{SQ} + k_\Delta[O_2(^3\Sigma)] - \left[\sqrt{\left(k_{GT} + f_s\left(\frac{N_{BF}}{N_A}\right)k_{SQ} + k_\Delta[O_2(^3\Sigma)]\right)^2 - 4f_s\left(\frac{N_{BF}}{N_A}\right)k_{GT}(k_{SQ} - 0.5k_{TT})}\right] \Big/ \left[2(k_{SQ} - 0.5k_{TT})\right] \quad (8)$$

Concentrations within an aggregate are scaled to the total suspension by multiplying the volume fraction of aggregates, V_r, the product of the volume of one aggregate, and the number of aggregates per volume of suspension n. The number of aggregates per volume of suspension, n, can be estimated by dividing the total number concentration (L^{-1}) of C$_{60}$ in the bulk N_B by the number of cages, N_F, per aggregate:

$$n = \frac{N_B}{N_F} \quad (9)$$

The volume fraction of the aggregates in the suspension (V_r) can then be calculated by multiplying n by the volume of each aggregate (eq 10).

$$V_r = \frac{\pi}{6} {d_f}^3 n \quad (10)$$

To address the transition from fractal to nonfractal behavior, we concatenate eqs 7 and 8 using a surface-weighted average of C$_{60}$ in suspension in calculating ROS generation:

$$[O_2(^1\Delta)] = ([T_1]_F V_r(1 - f_s) + [T_1]_S f_s)k_\Delta[O_2(^3\Sigma)]t \quad (11)$$

Molecules within the aggregate are subject to higher local concentrations of C$_{60}$ molecules making triplet−triplet annihilation and self-quenching reactions more likely. These molecules also have a lower chance of being photosensitized by irradiation. Finally, mass transfer of oxygen is also likely to be more limited within a larger fractal aggregate.

Table 1. Model Input Variables and Their Respective Standard Deviations

value	fullerene (C$_{60}$)	SD (σ)	fullerol (C$_{60}$(OH)$_{22-24}$)	SD (σ)
Φ_{GT}[4,21]	0.96[a]	0.04[a]	0.08[a]	0.08
k_{TT} (M^{-1} s^{-1})[21,22]	5.4×10^{9a}	5.0×10^8	5.4×10^9	5.0×10^9
k_{SQ} (M^{-1} s^{-1})[22]	1.8×10^{7a}	5.0×10^6	1.8×10^7	5.0×10^7
k_Δ (M^{-1} s^{-1})[4]	1.9×10^{9a}	2.0×10^{8a}	1.9×10^9	2.0×10^9
R (s^{-1})	0.1	0.05	0.1	0.05
D	2.8	0.2	2.3	0.2

[a] Numbers are known from literature.

Input Variables and Standard Deviations

Constants for these kinetic expressions have been measured experimentally utilizing C$_{60}$ molecules suspended in nonpolar solvents. For the purposes of this model, they serve as a basis for examining the efficacy of these calculations in aqueous systems. Moreover, the values for rate constants determined from these previous studies are taken to reflect the kinetics of homogeneous solutions of individual C$_{60}$ molecules and are assumed to apply to a potentially nonuniform distribution of C$_{60}$ within an aggregate in an aqueous suspension.

Table 1 lists the values for C$_{60}$ and C$_{60}$(OH)$_{22-24}$ parameters used to perform calculations of comparative ROS generation by aggregates of these two materials: quantum yield (Φ_{GT}), rate of triplet−triplet annihilation (k_{TT}), rate of self-quenching (k_{SQ}), rate of singlet oxygen formation (k_Δ), fractal dimension (D), and rate of optically induced transition effects (R). In the case of the underivatized C$_{60}$, the dominant pathway for energy transfer is intersystem crossing (see the Supporting Information); therefore, Φ_{GT} is nearly unity (0.96 ± 0.04).[4] Hydroxylation of the C$_{60}$ cage in the case of fullerol disturbs the conjugated π-bond cage, increases nontriplet forming pathways such as fluorescence,[20] and subsequently decreases the quantum yield. Therefore, the

(19) Badireddy, A. R.; Hotze, E. M.; Chellam, S.; Alvarez, P.; Wiesner, M. R. Inactivation of Bacteriophages via photosensitization of fullerol nanoparticles. *Environ. Sci. Technol.* **2007**, *41*, 6627.

(20) Guldi, D. M.; Asmus, K. D. Photophysical properties of mono- and multiply-functionalized fullerene derivatives. *J. Phys. Chem. A* **1997**, *101*, 1472.

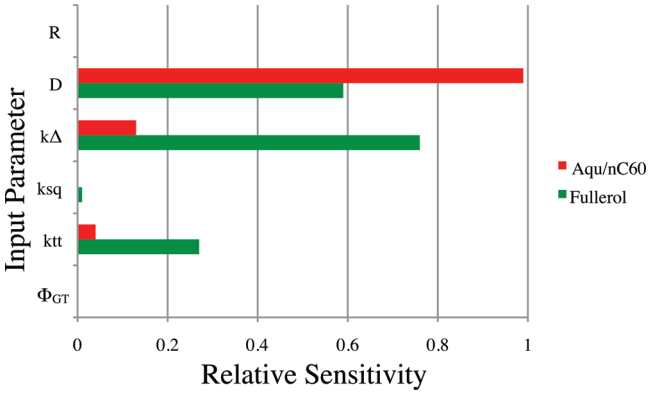

Figure 1. Pseudoglobal sensitivity values for the six model input variables: D, k_Δ, k_{SQ}, k_{TT}, QY, and R. The fractal dimension (D) has the largest effect on model output for aqu/nC_{60}, while the kinetic rate constant for reaction of triplet state with singlet oxygen (k_Δ) has the largest effect on fullerol model output.

value assumed for Φ_{GT} in the case of the fullerol (0.08) is approximately an order of magnitude lower than that for underivatized C_{60} and is based on spin trapping measurements of fullerol in D_2O.[21] Rate constants for k_{TT}, k_{SQ}, and k_Δ were measured for C_{60} suspended in a nonpolar solvent.[22] These rates are assumed to be the same for fullerol, since experimental measurements of these rates have not been made because the fullerol molecule is difficult to suspend individually. Similarly, standard deviations for these estimates were unknown for fullerol and were therefore set approximately 1 order of magnitude larger than those assumed for C_{60}. R is calculated based on measured intensity (I)[9] and absorption cross section (σ) values[23] and is not significantly different between C_{60} and fullerol given the high standard deviation that is assumed in part to account for scattering due to particles in suspension (see the Supporting Information). The last input variable, D, is estimated to be high (2.8 ± 0.2) for crystalline aqu/nC_{60} and lower (2.3 ± 0.2) for fullerol with a significant standard deviation for both particle aggregates.

Model Results and Discussion

A sensitivity analysis on the input variables for the model calculations was performed. Pseudoglobal sensitivity analysis is a tool that is commonly used to analyze chemical models involving multiple unknown reaction pathway contributions.[24] Sensitivities determine the relative strength of the relationship between an uncertain input and the output. Figure 1 plots pseudoglobal sensitivity values for both the aqu/nC_{60} and fullerol systems. This analysis leads to several important conclusions. First, wide ranges of uncertainty on the values for Φ_{GT} and R (originating for example from scattering due to aggregation of the C_{60} samples) can be tolerated without contributing to significant variability in the model calculations. Second, for aqu/nC_{60}, it is the fractal dimension of the aggregates and, by extension, aggregation state

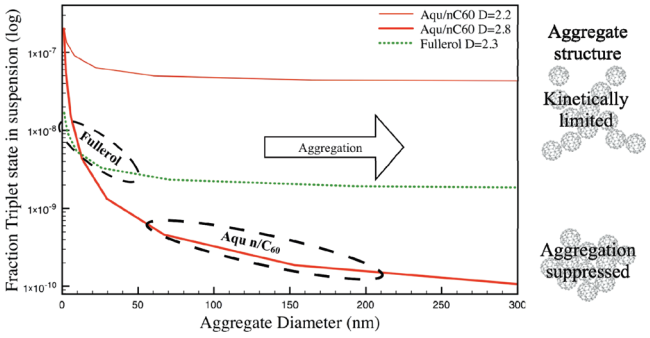

Figure 2. The red lines are the fraction of C_{60} cages in the triplet state [T_1] within the aqu/nC_{60} aggregate over a size range of 1−300 nm at two fractal dimensions (2.3 and 2.8). The green dashed line shows the percentage of fullerol cages in the triplet state [T_1] within an aggregate over a size range of 1−300 nm at a given fractal dimension (2.3). The dashed circled regions are the hypothesized ranges for diameters and fractal dimensions of aqu/nC_{60} and fullerol, respectively. Example kinetically limited (KL) and aggregation-suppressed (AS) structures are also illustrated.

that control the output of ROS. Third, ROS calculations for fullerol vary greatly as a function of rate constants associated with triplet state decay due to assumed high standard deviations (1 order of magnitude larger than the underivatized C_{60}). See the Supporting Information for more details.

The size and structure of nanoparticle aggregates in a suspension may vary based on hydrodynamics and solution conditions.[9,15,16] Fractal dimension (D) and aggregate diameter (d_f) were varied in calculations of the steady state fractions of triplet state C_{60} over a range of conditions encompassing those describing suspensions of aqu/nC_{60} and fullerol. A total concentration of 40 μM C_{60} was assumed for the suspensions in these calculations to allow for comparison with previously reported experiments.[9] A uniform concentration of 8.0 mg/L for the ground state oxygen ($[O_2(^3\Sigma)]$) is assumed for both the bulk suspension and within the aggregate. Similarly, mass-transport limitations on the diffusion of singlet oxygen out of the aggregate were assumed to be negligible in these calculations apart from the two-compartment assumption applied for C_{60} cages within aggregates ($[C_{60}]_F$) and those on the surface ($[C_{60}]_S$).

As previously noted in the context of sensitivity analysis, aggregate structure, as characterized by a given fractal dimension, D, is predicted to strongly affect the steady state fraction of triplet C_{60} within an aggregate. This is illustrated in Figure 2 where the steady state triplet fraction of C_{60} cages in a hypothetical fullerene aggregate has been calculated for two different fractal dimensions (D = 2.2 and 2.8). In a "looser" fractal aggregate (D = 2.2), a larger aggregate implies greater distances between C_{60} molecules (i.e., lower concentrations) in the aggregate and thus a higher percentage of C_{60} in the triplet state [T_1] and higher rates of ROS production. The limiting case corresponds to a suspension of individual, unaggregated C_{60} cages where ROS production is kinetically limited (KL) by the properties of an individual unaggregated cage. By comparison, the concentration of triplet state C_{60} present in a more compact (D = 2.8) aggregate (e.g., aqu/nC_{60}) is orders of magnitude lower when aggregates are large as the triplet state is rapidly quenched due to the proximity of neighboring C_{60} molecules and the limited number of these molecules on the surface of the aggregate. In this scenario, ROS production is suppressed by aggregation (AS). Conditions that might lead to disaggregation of the nC_{60} (e.g., interaction

(21) Zhao, B.; He, Y.; Bilski, P.; Chignell, C. Pristine (C_{60}) and hydroxylated [C_{60} (OH) $_{24}$] fullerene phototoxicity towards HaCaT keratinocytes: Type I vs Type II mechanisms. *Chem. Res. Toxicol.* **2008**, *21*, 1056.
(22) Ausman, K. D.; Weisman, R. B. Kinetics of fullerene triplet states. *Res. Chem. Intermed.* **1997**, *23*, 431.
(23) Belousov, V. P.; Belousova, I. M.; Gavronskaya, E. A.; Grigor'ev, V. A.; Danilov, O. B.; Kalintsev, A. G.; Krasnopol'skii, V. E.; Smirnov, V. A.; Sosnov, E. N. On the mechanism of optical limitation of laser radiation by fullerene-containing media. *Opt. Spectrosc.* **1999**, *87*, 772.
(24) Saltelli, A.; Ratto, M.; Tarantola, S.; Campolongo, F. Sensitivity analysis for chemical models. *Chem. Rev.* **2005**, *105*, 2811.

Table 2. Singlet Oxygen Production by Aggregates of aqu/nC$_{60}$ and Fullerol over 1 h for Different Aggregate Diameters[a]

size (nm)	aqu/nC$_{60}$ (D = 2.8) singlet oxygen (μM h^{-1})	fullerol (D = 2.3) singlet oxygen (μM h^{-1})
25	114	**229**
50	45.2	**176**
100	**20.0**	**147**
200	**9.83**	131
400	**5.39**	121

[a] Values in bold indicate most probable aggregate size ranges based on measurements.

with organic ligands[25] or hydroxylation perhaps catalyzed by singlet oxygen generation on the surface of nC$_{60}$[26]) will decrease the overall proximity of C$_{60}$ molecules in a given suspension, thereby leading to an increase in singlet oxygen production. The dashed green line in Figure 2 summarizes calculations of the fraction of triplet state cages predicted to be present in an aggregate consisting of hydrolxylated C$_{60}$ (fullerol) at fractal dimension 2.3. This fullerol curve shows that triplet states represent a larger fraction of primary molecules within the aggregates as opposed to triplet fraction within aqu/nC$_{60}$ (an order of magnitude less).

Comparison of the regions of predicted steady state triplet fractions for the fullerol and aqu/nC$_{60}$ suspensions demonstrates that structure will have a large effect on singlet oxygen output. When the concentrations of triplet state C$_{60}$ in the fullerol and aqu/nC$_{60}$ aggregates are translated into rates of singlet oxygen production, the production of singlet oxygen by aqu/nC$_{60}$ is predicted to be significantly lower than fullerol production (Table 2).

This is qualitatively consistent with experimental results where fullerol at 40 μM produced singlet oxygen at a rate of 1.9 μM h^{-1}, whereas aqu/nC$_{60}$ produced no detectable ROS under similar conditions (as measured by electron paramagnetic resonance, i.e., EPR).[9] The apparent paradox in ROS production by aqu/nC$_{60}$ and fullerol based on single molecule calculations is resolved in taking into account aggregation and noting that the tighter structure and larger size of aqu/nC$_{60}$ aggregates results in "aggregation-suppressed" ROS production, while the smaller, looser fullerol aggregates are "kinetically limited" with fewer opportunities for internal quenching of the triplet state that generate the ROS. Lower fractal dimensions lead to a greater fraction of cages on the surface, particularly as aggregate size decreases. "Kinetically limited" fullerol, with a fractal dimension near 2.3, has a higher f_s value at all diameters. Sensitivity analysis in Figure 1 demonstrates that kinetic input variables rather than structural ones are more sensitive for model output in the case of fullerol. "Aggregation-suppressed" aqu/nC$_{60}$, with a fractal dimension near 2.8, has a value of f_s that decreases rapidly with aggregate size, consistent with the calculated sensitivity to fractal dimension (Figure 1). Factors that determine structure and in particular surface fraction (D, d_f, d_p) must therefore be considered carefully in characterizing any system of aggregating nanoparticles.

While these calculations reflect the qualitative trends of singlet oxygen production in aqu/nC$_{60}$ versus fullerol, simplifying assumptions (e.g., no oxygen diffusion limitation) in this most parsimonious model do not allow for a quantitative match between theory and experimentally measured production by fullerol. The model predicts values 2 orders of magnitude higher than measured experimentally (176 $\gg$1.9 μM h^{-1}). Overestimation of ROS production may be attributed to an overestimation of k_Δ rate constants for the reaction of ground state oxygen with triplet state fullerol, the assumption of a uniform concentration of oxygen in and around the aggregates of fullerol (i.e., no mass transport limitations), and the oversimplification of mass transport and reactions such as those between singlet oxygen and the fullerene cages.

For example, recent studies suggest that singlet oxygen photosensitized by aggregated triplet fullerene cages can subsequently epoxidate the surfaces of those triplets.[26] Triplet state fullerol may also undergo this reaction. Using the rate constant (k_{TS}) for this reaction as a fitting coefficient to the experimental singlet oxygen generation rate ([$O_2(^1\Delta)$] = 1.9 μM h^{-1}), the value for singlet oxygen produced by 50 nm fullerol aggregates without this reaction is resolved with the observed value assuming that the total number of sites available on fullerol surfaces is large compared with those reacted (n_s = 5 per fullerol) (see the Supporting Information for more details).

$$[O_2(^1\Delta)] = V_r \frac{\left(\varepsilon k_\Delta [O_2(^3\Sigma)]\right)}{n_s k_{TS}} \left(1 - \exp(-n_s k_{TS} [T_1]_F t)\right) \quad (12)$$

The second order rate constant between singlet oxygen and triplet state fullerol (k_{TS}) is then estimated to be 1.63×10^7 M^{-1} s^{-1} when this function is fit to the data. This value is of the same order of magnitude as the self-quenching reaction rate constant (k_{SQ}), for a reaction between excited singlet and triplet states of fullerene, and is 1.8×10^7 M^{-1} s^{-1}. Furthermore, inclusion of this reaction increases differences in reactivity between aqu/nC$_{60}$ and fullerol assuming that undifferentiated C$_{60}$ molecules contain 5−6 more times singlet oxygen reaction sites.

Data from studies on aqueous fullerene ROS production confirm the utility of considering aggregation state as a primary indicator of reactivity.[7,9,27,28] Table 3 groups aggregates of C$_{60}$ according to study. Although detailed analyses of aggregate structure are not conducted in these studies, qualitative descriptors of aggregate structure are provided as a basis for determining whether ROS generation in the system is aggregation-suppressed (AS) or kinetically limited (KL). For example, UV−vis spectroscopy measurements with peak broadening between 400 and 500 nm indicate aggregation of C$_{60}$ primary particles.[29] In Table 3, C$_{60}$ aggregates producing the largest amount of singlet oxygen are given a relative production of 100% (●) while those suspensions producing no detectable ROS are indicated as ○ (0%). It is clear from these data that conditions favoring very small aggregates and or aggregates of lower fractal dimension correspond to higher measured ROS production, including cases where small aggregates are produced using surfactants or encapsulation agents. In contrast, suspensions produced by breaking down bulk crystalline C$_{60}$ or those produced in bottom-up precipitation from C$_{60}$ solutions in organic solvents produce little ROS due to the dense packing of crystalline structures in these latter suspensions.

These calculations and their pertinence to other recently published work on similar materials underscore the importance

(25) Chang, X.; Vikesland, P. J. Effects of carboxylic acids on nC$_{60}$ aggregate formation. *Environ. Pollut.* **2009**, *157*, 1072.
(26) Hou, W.-C.; Jafvert, C. T. Photochemical transformation of aqueous C$_{60}$ clusters in sunlight. *Environ. Sci. Technol.* **2009**, *43*, 362.
(27) Zhao, B. Z.; Bilski, P. J.; He, Y. Y.; Feng, L.; Chignell, C. F. Photo-induced reactive oxygen species generation by different water-soluble fullerenes (C$_{60}$) and their cytotoxicity in human keratinocytes. *Photochem. Photobiol.* **2008**, *84*, 1215.
(28) Lee, J.; Yamakoshi, Y.; Hughes, J. B.; Kim, J. H. Mechanism of C$_{60}$ photoreactivity in water: Fate of triplet state and radical anion and production of reactive oxygen species. *Environ. Sci. Technol.* **2008**, *42*, 3459.
(29) Fortner, J. D.; Lyon, D. Y.; Sayes, C. M.; Boyd, A. M.; Falkner, J. C.; Hotze, E. M.; Alemany, L. B.; Tao, Y. J.; Guo, W.; Ausman, K. D.; Colvin, V. L.; Hughes, J. B. C$_{60}$ in water: Nanocrystal formation and microbial response. *Environ. Sci. Technol.* **2005**, *39*, 4307.

Table 3. Data Summarized from Four Recent C_{60} Aggregate Photosensitization Studies

Type of Aggregate	Ref	Mean diameter (nm)	Size method	Modeling region[a]	Structure analysis	Relative $^1O_2$[b]
Aqu/nC_{60}	9	145	DLS	AS	High D predicted by XRD	○
Fullerol	9	200	DLS	KL	Low D predicted by XRD	●
Aqu/nC_{60}	7	100	DLS	AS	UV-Vis peak broadening	○
Son/nC_{60}	7	83	DLS	AS	UV-Vis peak broadening	○
Fullerol	7	n.g.	n.g.	KL	No UV-Vis peak broadening	◔
C_{60}/TX	7	< 10	DLS	AS	low UV-Vis peak broadening	●
C_{60}/Brij78	7	n.g.	n.g.	KL	low UV-Vis peak broadening	◕
THF/nC_{60}	27	60	TEM	AS	UV-Vis peak broadening	○
Son/nC_{60}	27	20	TEM	AS	UV-Vis peak broadening	○
(γ-CyD)2/C_{60}	27	n.g.	TEM	KL	Surfactant Stabilized	●
(γ-CyD/C_{60})	27	90	TEM	AS	UV-Vis peak broadening	○
Son/nC_{60}	28	n.g.	n.g.	AS	UV-Vis peak broadening	○
C_{60}/TX 100 (<c.m.c.)	28	n.g.	n.g.	AS	UV-Vis peak broadening	○
C_{60}/TX 100 (>c.m.c.)	28	n.g.	n.g.	KL	no UV-Vis peak broadening	●
C_{60}/SDBS (<c.m.c.)	28	n.g.	n.g.	AS	UV-Vis peak broadening	○
C_{60}/SDBS (>c.m.c.)	28	n.g.	n.g.	KL	low UV-Vis peak broadening	◕

[a] Modeling regions refer to theoretical trends suggesting either aggregation-suppressed (AS) or kinetically limited (KL) ROS production based. [b] Relative $^1O_2$ compares aggregates within each study with the symbol ● representing the highest production and the symbol ○ representing no detectable production.

of aggregate structure in determining nanoparticle reactivity. We anticipate that this theoretical framework will apply to describe aggregation-induced changes that may occur in other nanoparticle systems, such as hydroxyl radical forming semiconductors and some photoluminescing nanoparticles, where surface−surface interactions between nanoparticles may affect reactivity.

Supporting Information Available: Details of the model derivation, a description of the sensitivity analysis method, a discussion of possible sources of quantitative error in the model, as well as a list of equation variables and their corresponding units. This material is available free of charge via the Internet at http://pubs.acs.org.